Scientific Research Publishing

Open Journal of Applied Sciences, 2025, 15(4), 938-954
https://www.scirp.org/journal/ojapps
ISSN Online: 2165-3925
ISSN Print: 2165-3917

Dynamic Characteristics Analysis of Hollow Shafts Based on Higher Order Shear Theory

Zhichao Feng[1], Yancong Lin[2*], Penghui Qian[1], Zhenglong Dai[1], Shan Zeng[1], Fei Wang[2]

[1]School of Aerospace Engineering, Nanchang Hangkong University, Nanchang, China
[2]School of Power and Energy, Nanchang Hangkong University, Nanchang, China
Email: *nchufzc@163.com

How to cite this paper: Feng, Z.C., Lin, Y.C., Qian, P.H., Dai, Z.L., Zeng, S. and Wang, F. (2025) Dynamic Characteristics Analysis of Hollow Shafts Based on Higher Order Shear Theory. *Open Journal of Applied Sciences*, **15**, 938-954.
https://doi.org/10.4236/ojapps.2025.154063

Received: March 20, 2025
Accepted: April 7, 2025
Published: April 10, 2025

Abstract

This paper investigates the dynamic characteristics of hollow shaft rotor systems using a higher-order shear deformation theory (HOSDT). The authors based on the HOSDT and combined with the finite element method, a novel finite element model has been established, enabling rapid modeling and dynamic characteristic analysis of hollow shaft rotor system models with arbitrary dimensional parameters. And compare its performance with classical beam theories (Euler-Bernoulli and Timoshenko) and 3D solid element simulations in ANSYS. They analyze modal analysis, unbalanced response analysis, and stress computation. The results suggest that the HOSDT model offers superior accuracy compared to classical beam theories, especially for short, thick beams and thin-walled beams where shear effects are prominent, while also providing computational advantages over 3D solid element models. The study addresses the limitations of classical beam theories in accurately capturing shear effects in hollow shaft rotor systems, particularly in short, thick, and thin-walled scenarios. While 3D FEA can provide accurate results, it comes with high computational cost. The proposed HOSDT-based FEA model provides a balance between accuracy and computational efficiency. The application of HOSDT to hollow shafts and the comparative analysis with existing methods represent a valuable contribution.

Keywords

Hollow Shaft Rotor Systems, 1D Beam Theory, Higher Order Shear Theory, Dynamic Characteristics

1. Introduction

Rotor-bearing systems play an indispensable role in daily life and industrial production, with applications spanning automotive transmission systems, industrial

steam turbines, and aerospace engineering. In many mechanical structures, the shaft within a rotor system serves as a critical component that integrates the entire system. During operation, it supports other parts, transmits power, and ensures mechanical functionality. Shaft failure can destabilize interconnected components, leading to systemic breakdowns and potentially severe consequences. Moreover, rotor systems inherently generate vibrations during operation, which directly impact shaft stability. Notably, when the system reaches its critical speed, resonance phenomena may induce intense vibrations. Accurately analyzing the dynamic characteristics of rotor systems, mitigating resonance-induced vibrations, and enhancing system stability are therefore crucial for optimizing shaft design and ensuring operational reliability.

Over the past few decades, the application of finite element technology has significantly enhanced mechanical design efficiency. It not only improves the reliability of mechanical component design but also reduces workload and lowers costs. However, when performing 3D simulations of stepped shafts using solid elements, the computational complexity often leads to slow processing and convergence challenges, particularly under complex boundary conditions. To mitigate this, beams are frequently simplified as 1D problems. Classical beam theories such as Euler-Bernoulli beam theory and Timoshenko beam theory are commonly employed.

In Euler-Bernoulli beam theory, cross-sections perpendicular to the neutral axis before deformation remain planar and orthogonal to the deformed axis afterward. Since this theory neglects shear deformation and rotational inertia effects, it performs well in low-frequency analyses but encounters limitations at higher frequencies. Consequently, the Euler-Bernoulli model is suitable only for slender beams with negligible shear effects and fails to accurately predict the behavior of short or thick beams.

Timoshenko beam theory, another widely used approach, accounts for shear deformation by relaxing the assumption of cross-sectional orthogonality to the deformed axis. By incorporating shear stress and rotational inertia, it better captures the dynamics of short beams, laminated beams, and high-frequency excitations where wavelengths are comparable to beam thickness. Despite extensive refinements by researchers globally, Timoshenko beam theory still faces numerical challenges such as shear locking, which artificially reduces structural deformation and compromises result accuracy.

To address these limitations, higher order shear beam theories have been developed based on advanced shear deformation assumptions. These theories eliminate the need for shear correction factors while naturally satisfying the boundary condition of zero surface shear stress, thereby avoiding shear locking. Their advantages include refined modeling of shear deformation and rotational inertia, making them robust for both static and dynamic analyses.

Among early scholars who pioneered higher order shear theory, the contributions of Reissner and Levinson are particularly noteworthy. Reissner [1] [2] de-

veloped a theory for bending analysis by incorporating the influence of transverse shear on deformation. His work addressed stress concentration errors in classical theories under simply supported edge conditions, demonstrating superior accuracy. Later in 1981, Levinson [3] proposed a novel theory assuming cubic variation of cross-sectional displacement along the beam axis, enabling advanced mechanical analysis of rectangular beams via higher order shear deformation principles. This theoretical framework has since attracted extensive research and practical applications: Huang and Li [4] applied higher order shear beam theory to radially heterogeneous circular beams, analyzing transverse bending and vibrations. To capture bending responses in complex cross-sections, Choi and Kim [5] formulated a higher order theory for thin-walled rectangular hollow beams, validating its efficacy in vibration and buckling analyses. Nguyen *et al.* [6] resolved significant sectional deformation issues at beam-shell junctions in finite element models by integrating higher order beam elements with shell elements, achieving precise predictions for thin-walled composite structures. Ziou *et al.* [7] introduced a polynomial-based higher order shear deformation theory for static analysis of functionally graded material (FGM) beams. Müsevitoğlu *et al.* [8] investigated static behaviors of FGM beams using a novel finite element model derived from higher order shear theory, systematically evaluating stiffness coefficients across varying thicknesses and boundary conditions. Vinh [9] pioneered the application of higher order shear deformation theory to comprehensively study bending, vibration, and buckling in bidirectional FGM sandwich plates. Avcar *et al.* [10] developed a sandwich beam model based on higher order shear theory to quantify geometric effects on natural frequencies.

To more accurately analyze the dynamic characteristics of hollow shafts, this study establishes a finite element model for hollow shaft rotor systems based on higher order shear deformation theory. Compared to 3D solid element models, the proposed beam model offers significant advantages in computational speed. Furthermore, relative to classical 1D beam theory models, the higher order shear beam model developed herein demonstrates superior accuracy in dynamic analysis.

2. Beam Theory Formulation and Model Development

This chapter formulates the governing equations of classical beam theories and higher order shear beam theory through theoretical derivation. Based on the derived equations, a finite element model of the higher order shear beam is developed, enabling precise mechanical analysis.

2.1. Formulation of Classical Beam Theory Equations

The Euler-Bernoulli beam theory posits that cross-sections perpendicular to the neutral axis before deformation remain planar and perpendicular to the deformed neutral axis after bending, as illustrated in **Figure 1**.

The second moment of area for a hollow shaft with an annular cross-section is as follows

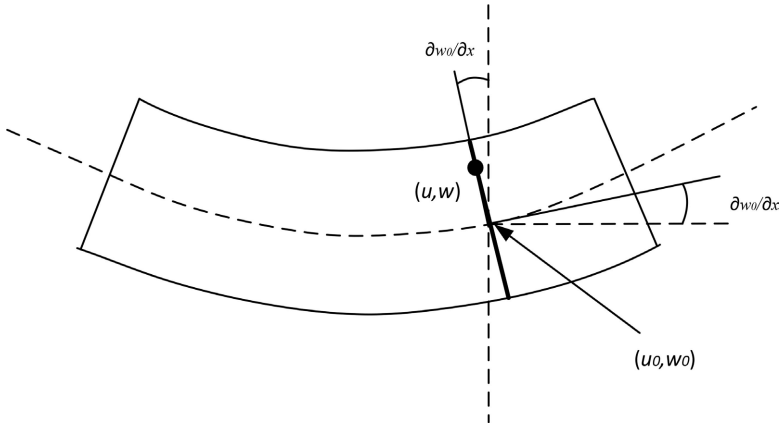

Figure 1. Schematic of Euler-Bernoulli beam theory.

$$I_z = \frac{\pi\left[\left(2r_o\right)^4 - \left(2r_i\right)^4\right]}{64} = \frac{\pi\left(r_o^4 - r_i^4\right)}{4} \tag{2-1}$$

The cross-sectional area is

$$A = \pi\left(r_o^2 - r_i^2\right) \tag{2-2}$$

The vibration governing equations of the Euler-Bernoulli beam theory are as follows

$$\begin{aligned} EI_z \frac{\partial^4 w(x,t)}{\partial x^4} + \rho A \frac{\partial^2 w(x,t)}{\partial t^2} &= 0 \\ \omega &= \left(\frac{n\pi}{L}\right)^2 \cdot \sqrt{\frac{EI_z}{\rho A}} \end{aligned} \tag{2-3}$$

In the equation, $w(x,t)$ is the transverse displacement of the beam at position x, n is the mode number, L is the length of the beam, E is the Young's modulus of the beam material, ρ is the density of the beam material, and ω is the natural frequency of the beam.

Unlike the Euler-Bernoulli beam theory, Timoshenko beam theory accounts for the effects of shear deformation, as illustrated in Figure 2.

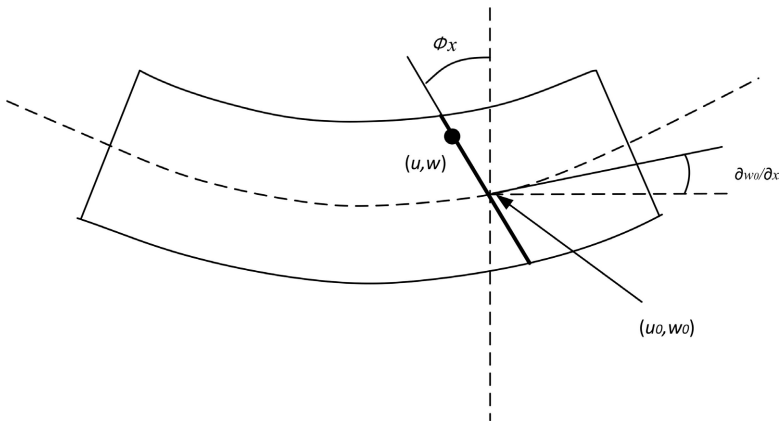

Figure 2. Schematic of Timoshenko beam theory.

The governing equations of the Timoshenko beam theory are Equation (2-4).

$$\begin{aligned} &EI_z\frac{\partial^4 w(x,t)}{\partial x^4}+\rho A\frac{\partial^2 w(x,t)}{\partial t^2}-k_s GA\left(\frac{\partial^2 w(x,t)}{\partial x^2}-\frac{\partial \psi(x,t)}{\partial x}\right)=q(x,t) \\ &k_s GA\left(\frac{\partial w(x,t)}{\partial x}-\psi(x,t)\right)=0 \end{aligned} \tag{2-4}$$

In the equations, G is the shear modulus of the beam material, k_s is the shear coefficient for the Timoshenko beam, and $q(x,t)$ is the uniformly distributed load per unit length on the beam. The first equation describes the coupling relationship between the bending and transverse vibration of the beam and shear deformation; the second equation reflects the relationship between shear deformation and the rotation angle.

2.2. Formulation of Higher Order Shear Beam Theory Equations

The schematic diagrams of the hollow shaft model and its differential element established based on the higher order shear deformation theory in this paper are shown in Figure 3. The outer diameter of the shaft is r_o, the inner diameter is r_i, and the length is L.

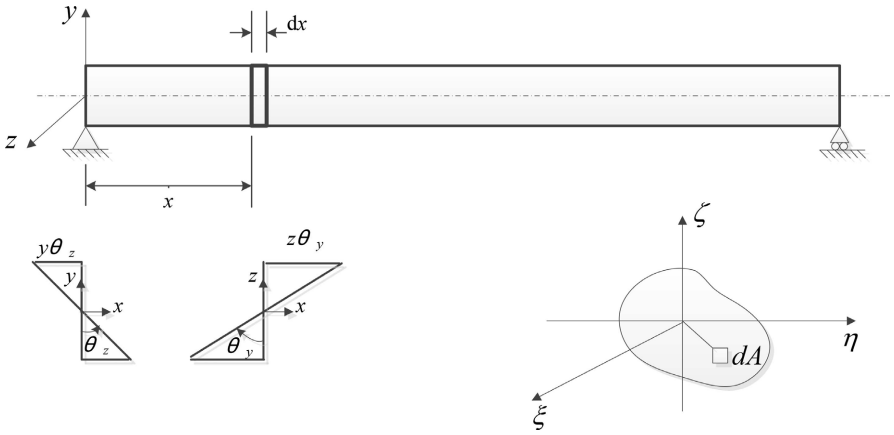

Figure 3. Schematic of higher order beam theory.

For a hollow circular cross-sectional beam under transverse bending, the shear stress (shear strain) at any boundary of the inner and outer circumferences is zero In the cylindrical coordinate system, the shear strain between the axial and radial directions is expressed as

$$\varepsilon_{rx}=\frac{1}{2}\left(\frac{\partial u_r}{\partial x}+\frac{\partial u_x}{\partial r}\right)=\frac{1}{2r}\left(y\frac{\partial u_y}{\partial x}+z\frac{\partial u_z}{\partial x}+y\frac{\partial u_x}{\partial y}+z\frac{\partial u_x}{\partial z}\right) \tag{2-5}$$

The displacement field is

$$\begin{aligned} u_x&=\psi(y,z)v'(x)+\vartheta(y,z)w'(x)-\left[\psi(y,z)+y\right]\theta_z(x)+\left[\vartheta(y,z)+z\right]\theta_y(x) \\ u_y&=v \\ u_z&=w \end{aligned} \tag{2-6}$$

where

$$\vartheta(y,z)=\frac{y^4z}{5r_i^2r_o^2}+\frac{2y^2z^3}{5r_i^2r_o^2}-\frac{y^2z\left(r_i^2+r_o^2\right)}{3r_i^2r_o^2}+\frac{z^5}{5r_i^2r_o^2}-\frac{z^3\left(r_i^2+r_o^2\right)}{3r_i^2r_o^2}$$
$$\psi(y,z)=\frac{y^5}{5r_i^2r_o^2}+\frac{2y^3z^2}{5r_i^2r_o^2}-\frac{y^3\left(r_i^2+r_o^2\right)}{3r_i^2r_o^2}+\frac{yz^4}{5r_i^2r_o^2}-\frac{yz^2\left(r_i^2+r_o^2\right)}{3r_i^2r_o^2} \quad (2\text{-}7)$$

Assuming the secondary stress components ($\sigma_{yy},\sigma_{zz},\sigma_{yz}$) to be negligible, the constitutive equations of the beam model can be expressed as

$$\begin{aligned}\sigma_{xx}&=E\varepsilon_{xx}\\ \sigma_{xz}&=2G\varepsilon_{xz}\\ \sigma_{yz}&=2G\varepsilon_{yz}\end{aligned} \quad (2\text{-}8)$$

In the equation, E is the Young's modulus of the material, and G is the shear modulus of the material. The expressions for the strain components are

$$\varepsilon_{ij}=\frac{1}{2}\left(u_{i,j}+u_{j,i}\right),(i,j)=(x,y,z) \quad (2\text{-}9)$$

The strain energy density is

$$U_e=\frac{1}{2}\sigma_{ij}\varepsilon_{ij}=\frac{1}{2}\left(\sigma_{xx}\varepsilon_{xx}+2\sigma_{xy}\varepsilon_{xy}+2\sigma_{xz}\varepsilon_{xz}\right) \quad (2\text{-}10)$$

The total kinetic energy of the beam is

$$T=\frac{1}{2}\int_0^L\left[m\dot{v}^2+m\dot{w}^2-2J_p\Omega\theta_y\dot{\theta}_z+J_p\Omega^2+J_d\dot{\theta}_y^2+J_d\dot{\theta}_z^2\right]\mathrm{d}x \quad (2\text{-}11)$$

The equilibrium equations constructed are as Equation (2-12)

$$\begin{aligned}&\delta(v):m\ddot{v}+EI_6v^{(4)}+EI_{46}\theta_z^{(3)}-\frac{1}{2}G\tilde{A}v''+\frac{1}{2}G\tilde{A}\theta_z'=0\\ &\delta(w):m\ddot{w}+EI_6w^{(4)}-EI_{46}\theta_y^{(3)}-\frac{1}{2}G\tilde{A}w''-\frac{1}{2}G\tilde{A}\theta_y'=0\\ &\delta(\theta_z):-J_p\Omega\dot{\theta}_y+J_d\ddot{\theta}_z-EI_{46}v^{(3)}-E\tilde{I}_2\theta_z''-\frac{1}{2}G\tilde{A}v'+\frac{1}{2}G\tilde{A}\theta_z=0\\ &\delta(\theta_y):J_p\Omega\dot{\theta}_z+J_d\ddot{\theta}_y+EI_{46}w^{(3)}-E\tilde{I}_2\theta_y''+\frac{1}{2}G\tilde{A}w'+\frac{1}{2}G\tilde{A}\theta_y=0\end{aligned} \quad (2\text{-}12)$$

where

$$\begin{aligned}\frac{1}{2}G\tilde{A}&=-\frac{14}{27}G\pi r_i^2-\frac{76G\pi r_i^6}{3375r_o^4}+\frac{22G\pi r_i^4}{135r_o^2}+\frac{14}{27}G\pi r_o^2-\frac{22G\pi r_o^4}{135r_i^2}+\frac{76G\pi r_o^6}{3375r_i^4}\\ E\tilde{I}_2&=-\frac{11}{72}\pi r_i^4E-\frac{7\pi r_i^8E}{1800r_o^4}+\frac{7\pi r_i^6E}{150r_o^2}+\frac{11}{72}\pi r_o^4E-\frac{7\pi r_o^6E}{150r_i^2}+\frac{7\pi r_o^8E}{1800r_i^4}\\ EI_{46}&=-\frac{1}{24}\pi r_i^4E+\frac{7\pi r_i^8E}{1800r_o^4}-\frac{29\pi r_i^6E}{1800r_o^2}+\frac{1}{24}\pi r_o^4E+\frac{29\pi r_o^6E}{1800r_i^2}-\frac{7\pi r_o^8E}{1800r_i^4}\\ EI_6&=-\frac{1}{72}\pi r_i^4E-\frac{7\pi r_i^8E}{1800r_o^4}-\frac{13\pi r_i^6E}{900r_o^2}+\frac{1}{72}\pi r_o^4E+\frac{13\pi r_o^6E}{900r_i^2}+\frac{7\pi r_o^8E}{1800r_i^4}\end{aligned} \quad (2\text{-}13)$$

2.3. Development of the Higher Order Shear Beam Model

The general methodology for developing the 1D simplified beam model in this study is illustrated in Figure 4.

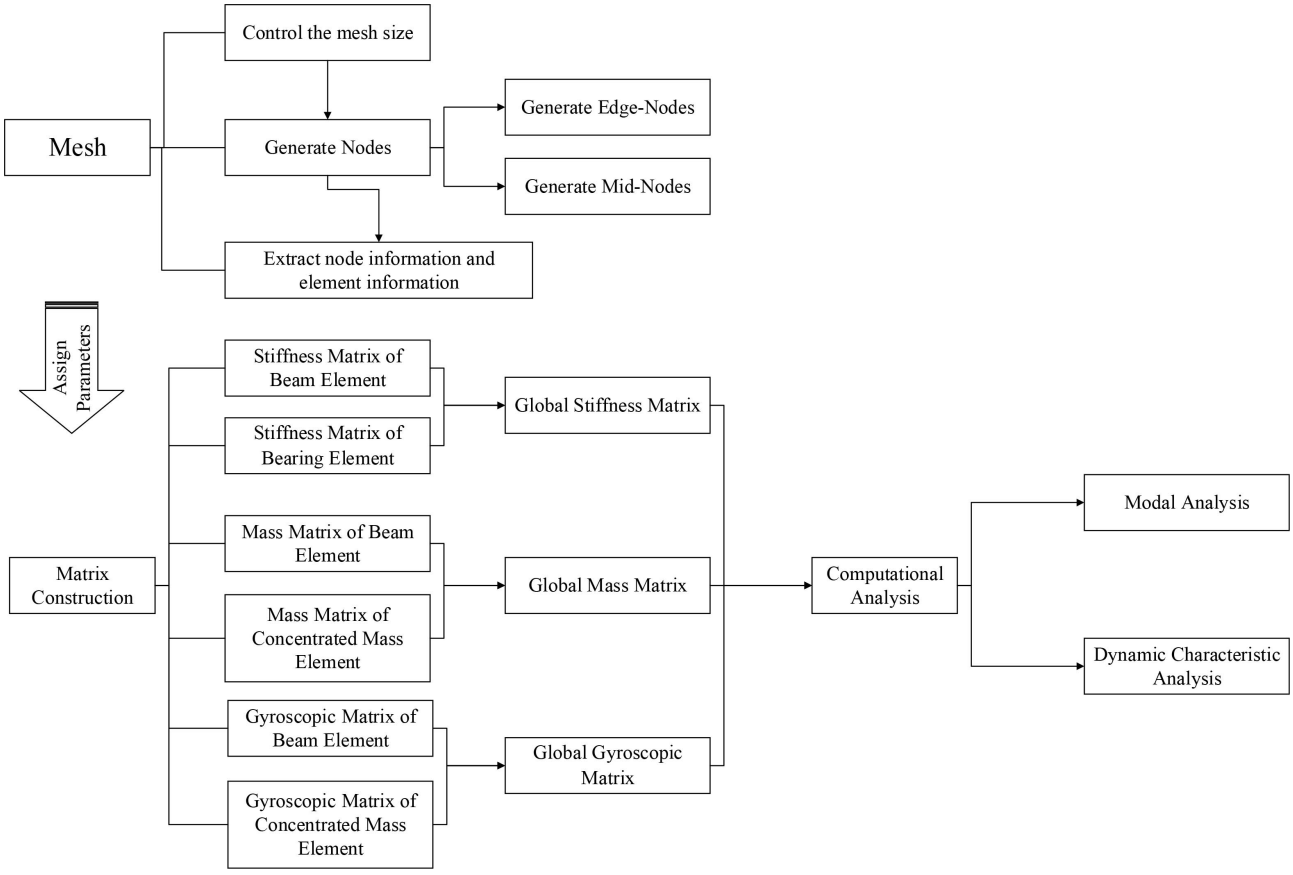

Figure 4. Flowchart of the construction process of the higher order shear deformation beam model.

This paper combines theoretical calculations with the finite element method, employs a three-node finite element method to establish a higher order shear beam model, where each node possesses four degrees of freedom (denoted as v, u, θ_y, θ_z). The element matrices are formulated based on the beam equilibrium equations. Let the total number of nodes be n, the degree-of-freedom array of the beam model can then be expressed as

$$\left[v_1, u_1, \theta_{y1}, \theta_{z1}, v_2, u_2, \theta_{y2}, \theta_{z2}, \cdots, v_n, u_n, \theta_{yn}, \theta_{zn}\right] \tag{2-14}$$

The global system matrix has a dimension of $4n \times 4n$. By mapping the degrees of freedom (DOF) numbering, the positions of the element matrices within the global system matrix can be determined. Assemble the global stiffness matrix, global mass matrix, and global gyroscopic matrix to establish a finite element model of a hollow shaft rotor system using higher order shear beam elements, which can easily achieve parameter settings for hollow shaft rotor systems of arbitrary dimensions.

3. Dynamic Characteristics Analysis and Model Validation of Hollow Shaft Rotor Systems

This chapter utilizes the higher order shear beam model established in the previous chapter to analyze the dynamic characteristics of a constant cross-section hol-

low shaft. The results are compared with those obtained from classical beam theory and commercial finite element software ANSYS. This comparative analysis demonstrates the accuracy and reliability of the proposed methodology.

3.1. Static Modal Analysis

This paper employs the state-space method to calculate the modal characteristics of a higher order shear hollow shaft rotor system. The analysis begins by establishing the dynamic model of the rotor system.

$$\{M\}\{\ddot{x}\}+\{C\}\{\dot{x}\}+\{K\}\{x\}=\{0\} \tag{3-1}$$

In the equation, M is the element mass matrix, C is the element damping matrix, K is the element stiffness matrix, and x is the axial displacement of the node. By solving the full matrix v and the diagonal matrix d of $\{M\},\{K\}$, the mode shapes and natural frequencies of the rotor system can be calculated.

The hollow shaft rotor system model was established using 45 steel for numerical analysis, with the specific dimensional parameters and material parameters of the model listed in Table 1.

Table 1. Parameter settings for the hollow shaft rotor system model.

Parameter Name	Parameter Settings
Elastic Modulus (E)	200 GPa
Density (ρ)	7850 kg/m^3
Poisson's Ratio (ε)	0.3
Stiffness of Support 1	1×10^{10} N/m
Stiffness of Support 2	1×10^{10} N/m

First, a mesh independence verification was performed for the Solid186 element model by establishing the hollow shaft rotor system as shown. Due to the thin-walled structure of the hollow shaft, the element size is influenced by the wall thickness. Therefore, this section defines the element size based on the number of element layers across the hollow shaft wall (calculated as (outer diameter − inner diameter)/number of element layers) for mesh independence verification. Different element sizes were configured to achieve varying numbers of element layers in the hollow shaft. Static modal analysis was conducted on the hollow shaft, and the first-order natural frequencies under different element sizes were recorded. Using three-layer solid elements as the reference, errors for different element sizes were calculated, as illustrated in Figure 5. According to the mesh independence verification results: although three-layer solid elements in the thin-walled hollow shaft demonstrate higher accuracy, the computational time is significantly longer. In contrast, two-layer solid elements provide faster computation with equally minimal errors. Consequently, the finite element calculations for the hollow shaft in this study adopt a two-layer solid element configuration for mesh sizing (Figure 6).

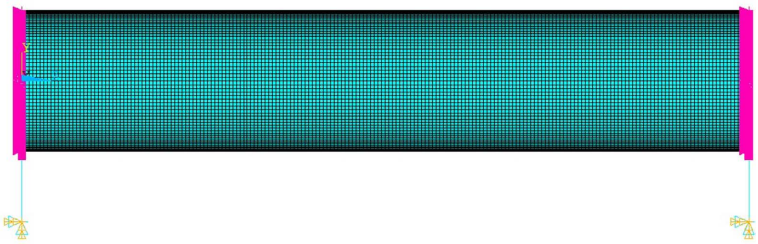

Figure 5. Finite element model of a hollow shaft rotor system.

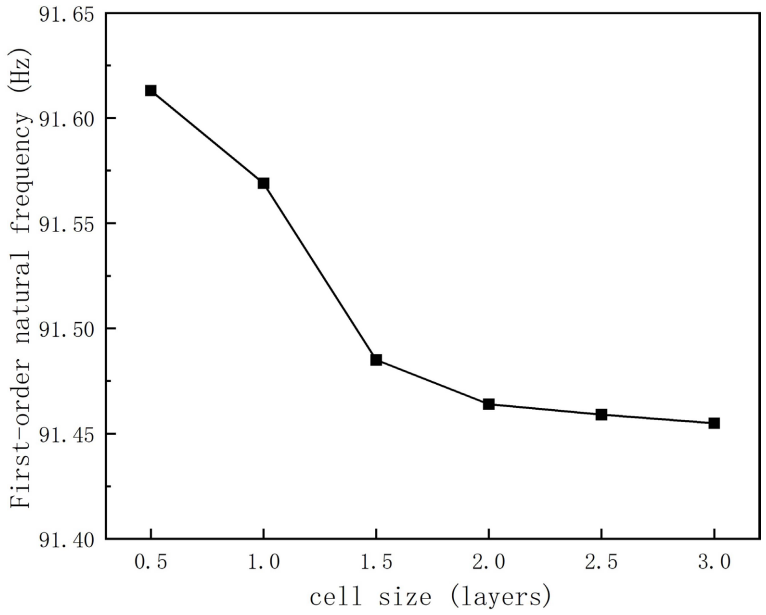

Figure 6. Line chart of mesh size versus static modal analysis results.

The inner diameter of the hollow shaft rotor system is fixed at 45 mm, and the outer diameter is fixed at 50 mm. Static modal calculations are performed for hollow shaft rotor systems with different length-to-diameter ratios, and the resulting curves and numerical results are presented in **Table 2** and **Figure 7**. The computation time was recorded: the Solid186 element finite element method took approximately 30 minutes, while the higher-order shear beam element and Timoshenko beam element methods required similar time, only around 20 seconds, the computational efficiency is significantly higher than that of the Solid186 element model. Then, the results show that for smaller length-to-diameter ratios, the computational errors between the higher order shear beam model and the Timoshenko beam model are comparable. However, as the length-to-diameter ratio increases, the error of the Timoshenko beam model rises to 14.91%, while the higher order shear beam model maintains high accuracy. This demonstrates the computational accuracy advantage of the proposed higher order shear beam model over traditional beam models. For rotor systems with small length-to-diameter ratios, the Euler-Bernoulli beam theory neglects shear effects, leading to significant computational errors. Therefore, the results from Euler-Bernoulli beam theory are excluded in the analysis of short, thick beams in this study.

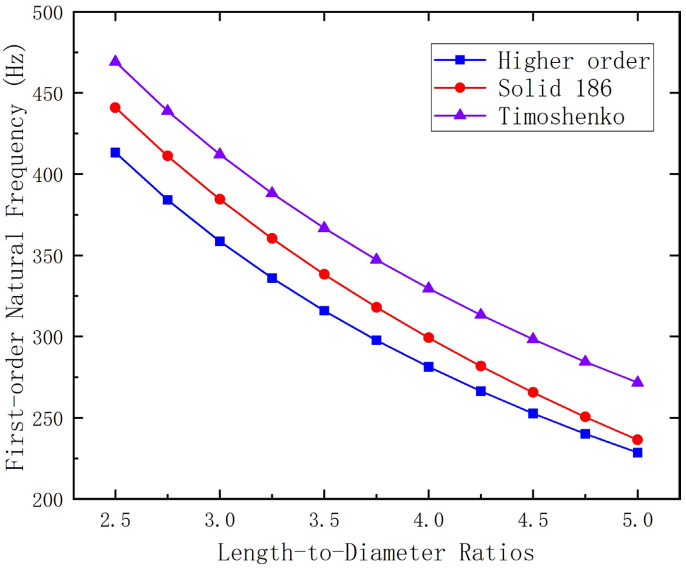

Figure 7. Curves of fundamental frequency calculation results from beam theories under different length-to-diameter ratios.

Table 2. Comparison of numerical results for fundamental frequency (Hz) from beam theories under different length-to-diameter ratios.

Length-to-Diameter Ratio	Calculation Results of Solid186 Element	Calculation Results of Timoshenko Beam		Calculation Results of Higher Order	
	Numerical Results	Numerical Results	Relative Error	Numerical Results	Relative Error
2.5	440.933	469.065	6.38%	413.272	6.27%
2.75	411.150	438.780	6.72%	384.118	6.57%
3	384.491	412.039	7.16%	358.595	6.74%
3.25	360.347	388.188	7.73%	336.016	6.75%
3.5	338.283	366.729	8.41%	315.857	6.63%
3.75	317.982	347.284	9.22%	297.725	6.37%
4	299.209	329.554	10.14%	281.304	5.98%
4.25	281.787	313.301	11.18%	266.357	5.48%
4.5	265.581	298.333	12.33%	252.672	4.86%
4.75	250.481	284.491	13.58%	240.098	4.15%
5	236.399	271.646	14.91%	228.493	3.34%

A further comparative analysis is conducted on the influence of other dimensional parameters. With the length-to-diameter ratio of the hollow shaft fixed, the outer diameter set to 50 mm, and the shaft length set to 2.5 m, the inner diameter of the hollow shaft is varied to investigate the effect of the inner-to-outer diameter ratio on the computational results. These results are summarized in Table 3 and Figure 8. The computation time was recorded: the Solid186 element finite element method took approximately 45 minutes, while the higher-order shear beam ele-

ment and Timoshenko beam element methods required similar time, only around 30 seconds. Then, the calculations reveal that when the inner-to-outer diameter ratio is small (thick-walled beams), the accuracy of the higher order shear beam model is comparable to that of the Timoshenko beam model. However, as the diameter ratio increases, the computational error of the Timoshenko beam model gradually grows, while the higher order shear beam model retains high precision. This demonstrates the clear computational advantage of the proposed higher order shear beam element in analyzing thick-walled beam structures.

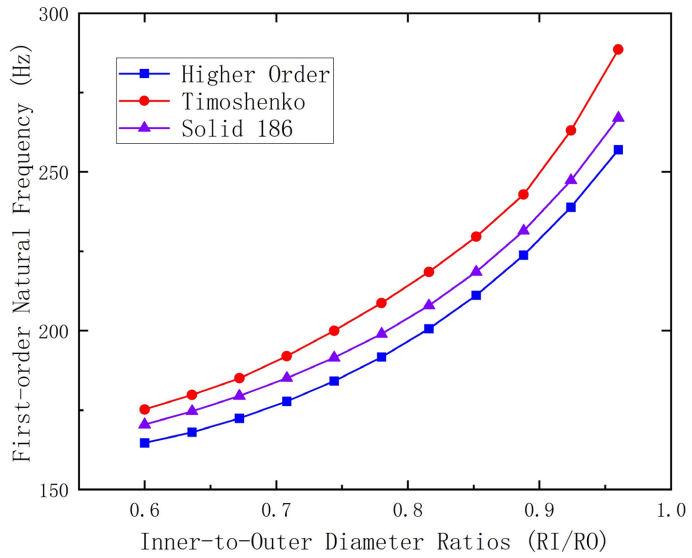

Figure 8. Curves of fundamental frequency calculation results from beam theories under different inner-to-outer diameter ratios.

Table 3. Comparison of numerical results for fundamental frequency (Hz) from beam theories under different inner-to-outer diameter ratios.

Inner-to-Outer Ratio	Calculation Results of Solid186 Element	Calculation Results of Timoshenko Beam		Calculation Results of Higher Order	
	Numerical Results	Numerical Results	Relative Error	Numerical Results	Relative Error
0.6	170.457	175.208	2.79%	164.692	3.38%
0.636	174.641	179.795	2.95%	168.039	3.78%
0.672	179.439	185.036	3.12%	172.392	3.93%
0.708	185.089	192.035	3.75%	177.749	3.97%
0.744	191.515	199.994	4.43%	184.154	3.85%
0.78	198.961	208.746	4.92%	191.713	3.64%
0.816	207.916	218.503	5.09%	200.628	3.51%
0.852	218.526	229.596	5.07%	211.181	3.36%
0.888	231.465	242.870	4.93%	223.763	3.33%
0.924	247.345	263.029	6.34%	238.880	3.42%
0.96	266.973	288.541	8.08%	256.979	3.74%

3.2. Unbalance Response Analysis

In rotor systems, due to factors such as manufacturing inaccuracies, the mass distribution of the rotor cannot achieve perfect rotational symmetry. Consequently, an offset of the center of mass generates centrifugal forces, which induce vibrations in the system. Unbalance response analysis is critical for implementing effective engineering measures to mitigate the effects of vibration, thereby enhancing the stability and reliability of the rotor system.

When considering the gyroscopic effect, the differential equation of motion for the rotor system is

$$\boldsymbol{M}\ddot{\boldsymbol{U}} + (\boldsymbol{C} + \boldsymbol{G})\dot{\boldsymbol{U}} + \boldsymbol{K}\boldsymbol{U} = \boldsymbol{F} \tag{3-2}$$

where, $\boldsymbol{M}$ is the element mass matrix, $\boldsymbol{C}$ is the element damping matrix, $\boldsymbol{G}$ is the gyroscopic matrix, $\boldsymbol{K}$ is the element stiffness matrix, is the unbalance force matrix, and $\boldsymbol{U}$ is the element displacement matrix, namely the unbalance response matrix.

Substituting the assumed solution with a concise $\boldsymbol{U} = \boldsymbol{U}_0 \mathrm{e}^{j\omega t}$ form into Equation (3-2) yields

$$\left(-\omega^2 \boldsymbol{M} + j\omega(\boldsymbol{C} + \boldsymbol{G}) + \boldsymbol{K}\right)\boldsymbol{U}_0 = \boldsymbol{F} \tag{3-3}$$

Thus, the unbalance response of the rotor system can be obtained

$$\boldsymbol{U} = \boldsymbol{U}_0 \mathrm{e}^{j\omega t} = \left(-\omega^2 \boldsymbol{M} + j\omega(\boldsymbol{C} + \boldsymbol{G}) + \boldsymbol{K}\right)^{-1} \boldsymbol{F} \mathrm{e}^{j\omega t} \tag{3-4}$$

A constant cross-section hollow shaft model is augmented with three concentrated masses located at the center of the rotor system, $0.2L$, and $0.8L$ along the shaft length (where L is the total shaft length). Each concentrated mass has a distinct unbalance magnitude, with specific parameters detailed in Table 4. Squeeze Film Dampers (SFD) are incorporated at both end supports, and their design parameters are provided in Table 5. Using the algorithm described in Section 2.2 of this paper, an unbalance response analysis of the rotor system is performed. The resulting unbalance response curves for the three concentrated masses are shown in Figure 9, and numerical results are summarized in Table 6. Compared with traditional ANSYS simulations, the proposed higher order shear beam element model demonstrates superior accuracy and reliability.

Table 4. Concentrated mass parameters of the hollow shaft rotor system.

	Mass (kg)	Rotational Inertia (kg·m²)	Unbalance (g·cm)
Concentrated Mass 1	10	12.5	0.1
Concentrated Mass 2	15	20	0.15
Concentrated Mass 3	20	30	0.2

Table 5. Parameter settings for SFD.

	Design Parameters
Dynamic Viscosity of Lubricating Oil μ	0.0117

Continued

Damper Radius R	50 mm
Damper Length l	50 mm
Radial Clearance of Damper h	1×10^{-3} m
Damper Support Stiffness K	1×10^{8} N/m

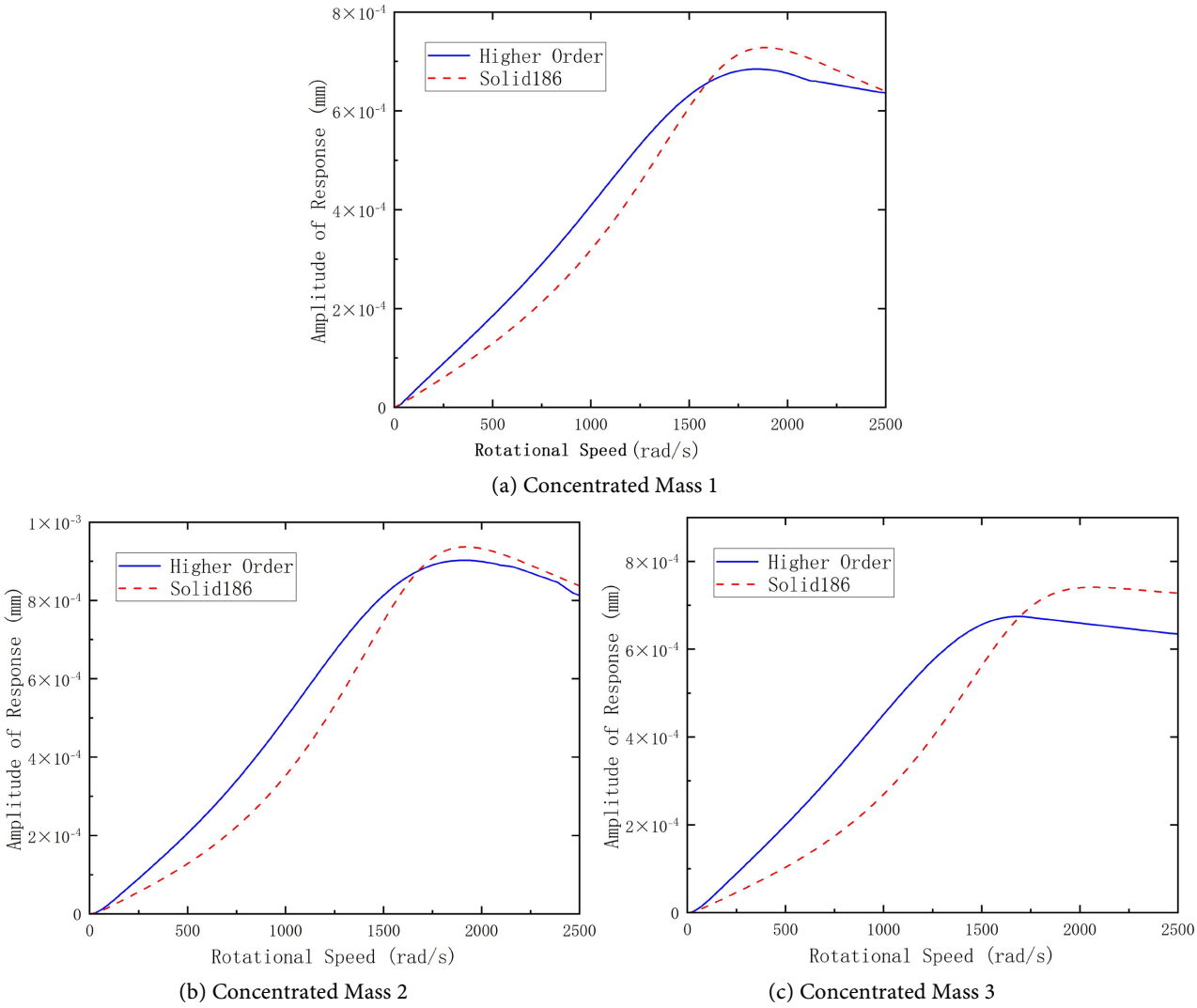

(a) Concentrated Mass 1

(b) Concentrated Mass 2

(c) Concentrated Mass 3

Figure 9. The imbalance response curve of the hollow shaft rotor system.

Table 6. The numerical results of the unbalance response of the hollow shaft rotor system.

	Amplitude of Response of Solid 186 Elements (mm)	Amplitude of Response of Higher Order Beam Elements (mm)	Relative Error
Concentrated Mass 1	7.430×10^{-4}	6.987×10^{-4}	5.96%
Concentrated Mass 2	9.365×10^{-4}	9.025×10^{-4}	3.63%
Concentrated Mass 3	7.411×10^{-4}	6.747×10^{-4}	8.96%

3.3. Calculation of Section Stress

In Chapter 2 of this paper, the formula for calculating element strain is derived,

and the formula for the radial stress of the element is expressed as

$$\sigma = E\varepsilon_{rx} = \frac{E}{2r}\left(y\frac{\partial u_y}{\partial x} + z\frac{\partial u_z}{\partial x} + y\frac{\partial u_x}{\partial y} + z\frac{\partial u_x}{\partial z} \right) \tag{3-5}$$

The rotor system is excited at its first critical speed, and an unbalance response analysis is performed to calculate the stress distribution in the hollow shaft rotor system when the response reaches its peak amplitude. The radial stress distribution data on the cross-sections of the three concentrated masses are extracted and visualized as contour plots, as shown in Figure 10. The contour plots reveal a symmetrical stress distribution, where the maximum radial stresses occur at the top and bottom ends of the hollow shaft with opposite directions, while the minimum stresses are observed near the central axis.

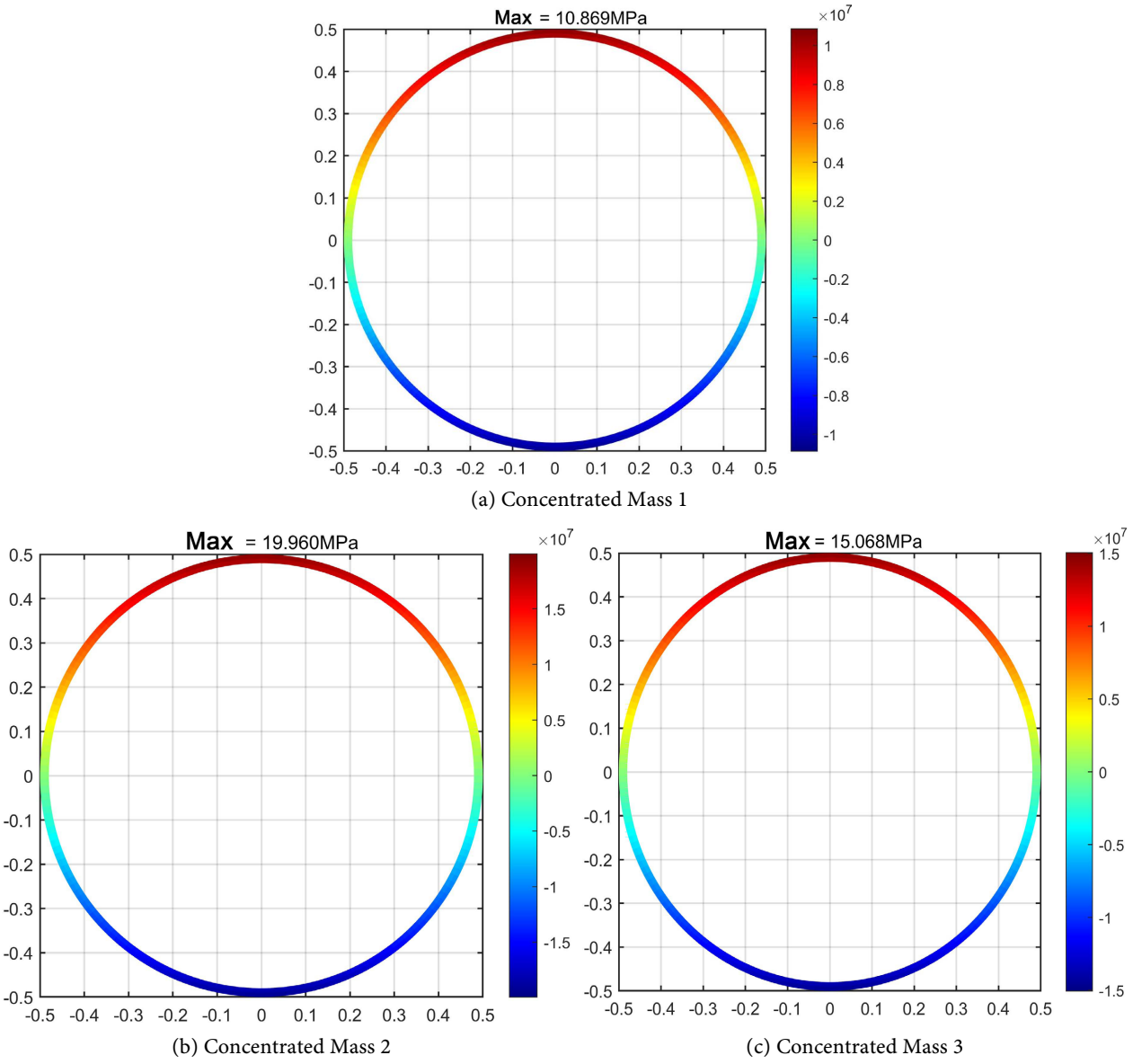

(a) Concentrated Mass 1

(b) Concentrated Mass 2

(c) Concentrated Mass 3

Figure 10. Contour plot of cross-sectional stress distribution at concentrated masses in the higher order shear beam element model.

In the finite element simulation model, identical support conditions are applied, and the rotor system is excited at its first critical speed to perform an unbalance response analysis. The radial stress distribution contour plots at the cross-sections of the three concentrated masses are obtained, as shown in Figure 11 with numerical results provided in Table 7. The results indicate that the stress distribution pattern closely resembles that of the higher order shear beam model, with stresses exhibiting symmetrical distribution. The calculated maximum radial stresses at the cross-sections of the three concentrated masses using both beam element models show strong consistency, validating the high precision of the proposed higher order shear beam element model in stress computation.

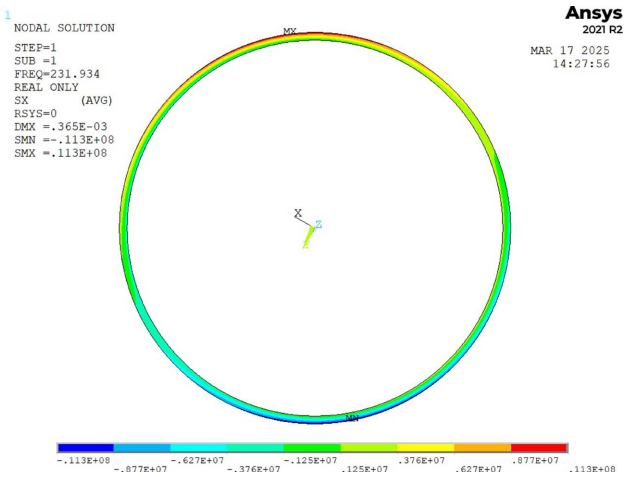

(a) Concentrated Mass 1

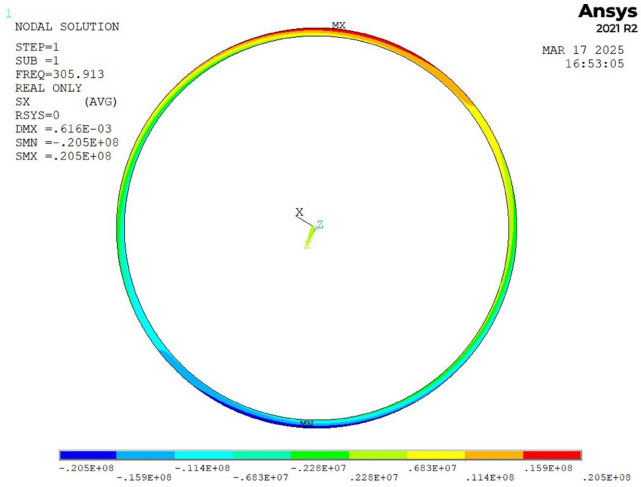

(b) Concentrated Mass 2

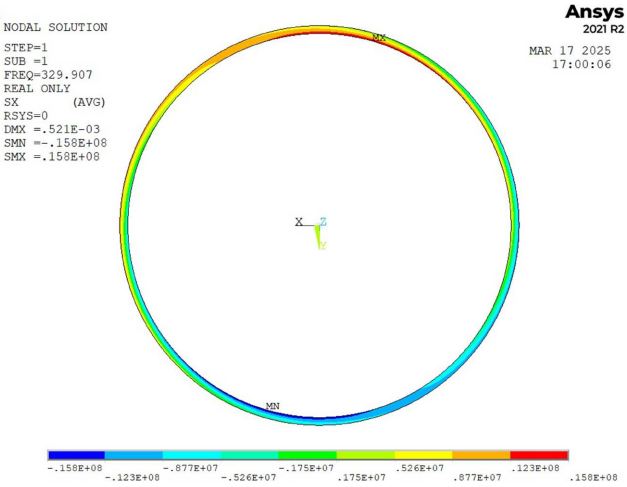

(c) Concentrated Mass 3

Figure 11. Contour plot of cross-sectional stress distribution at concentrated masses in the solid186 element model.

4. Conclusions

This study investigates the dynamic characteristics of rotor systems based on higher order shear beam theory, focusing on modal analysis, response analysis, and stress computation. The conclusions are summarized as follows:

Table 7. Numerical results of maximum radial stress (MPa) at cross-sections.

	Higher Order Beam Elements	Solid186 Elements	Relative Error
Concentrated Mass 1	10.869	11.279	3.64%
Concentrated Mass 2	19.960	20.476	2.52%
Concentrated Mass 3	15.068	15.779	4.51%

1) For short, thick beams with small length-to-diameter ratios, both the higher order shear beam model and the Timoshenko beam model exhibit high computational accuracy. However, as the length-to-diameter ratio increases or the wall thickness decreases, the influence of shear effects becomes more pronounced. Under these conditions, the computational error of the Timoshenko beam model grows significantly, while the higher order shear beam model retains sufficient accuracy.

2) Compared with solid element simulations in the commercial finite element software ANSYS, the proposed higher order shear beam element model achieves high precision and reliability in calculating the dynamic characteristics of rotor systems, while also demonstrating superior computational efficiency.

3) The proposed higher order shear beam element model significantly improves the computational accuracy and design efficiency for analyzing the dynamic behavior of hollow shaft rotor systems. This advancement provides a robust theoretical foundation for the structural design and optimization of rotor systems.

Conflicts of Interest

The authors declare no conflicts of interest regarding the publication of this paper.

References

[1] Reissner, E. (1945) The Effect of Transverse Shear Deformation on the Bending of Elastic Plates. *Journal of Applied Mechanics*, **12**, A69-A77. https://doi.org/10.1115/1.4009435

[2] Reissner, E. (1975) On Transverse Bending of Plates, Including the Effect of Transverse Shear Deformation. *International Journal of Solids and Structures*, **11**, 569-573. https://doi.org/10.1016/0020-7683(75)90030-x

[3] Levinson, M. (1981) A New Rectangular Beam Theory. *Journal of Sound and Vibration*, **74**, 81-87. https://doi.org/10.1016/0022-460x(81)90493-4

[4] Huang, Y. and Li, X. (2010) Bending and Vibration of Circular Cylindrical Beams with Arbitrary Radial Nonhomogeneity. *International Journal of Mechanical Sciences*, **52**, 595-601. https://doi.org/10.1016/j.ijmecsci.2009.12.008

[5] Choi, S. and Kim, Y.Y. (2021) Higher-Order Beam Bending Theory for Static, Free Vibration, and Buckling Analysis of Thin-Walled Rectangular Hollow Section Beams. *Computers & Structures*, **248**, Article ID: 106494. https://doi.org/10.1016/j.compstruc.2021.106494

[6] Nguyen, N., Jang, G., Choi, S., Kim, J. and Kim, Y.Y. (2018) Analysis of Thin-Walled Beam-Shell Structures for Concept Modeling Based on Higher-Order Beam Theory. *Computers & Structures*, **195**, 16-33.

https://doi.org/10.1016/j.compstruc.2017.09.009

[7] Ziou, H., Guenfoud, M. and Guenfoud, H. (2021) A Simple Higher Order Shear Deformation Theory for Static Bending Analysis of Functionally Graded Beams. *Jordan Journal of Civil Engineering*, 15, 209-224.

[8] Müsevitoğlu, A., Özütok, A. and Reddy, J.N. (2025) Static Analysis of Functionally Graded and Laminated Composite Beams Using Various Higher-Order Shear Deformation Theories: A Study with Mixed Finite Element Models. *European Journal of Mechanics—A/Solids*, **111**, Article ID: 105596. https://doi.org/10.1016/j.euromechsol.2025.105596

[9] Vinh, P.V. (2021) Analysis of Bi-Directional Functionally Graded Sandwich Plates via Higher-Order Shear Deformation Theory and Finite Element Method. *Journal of Sandwich Structures & Materials*, **24**, 860-899. https://doi.org/10.1177/10996362211025811

[10] Avcar, M., Hadji, L. and Civalek, Ö. (2021) Natural Frequency Analysis of Sigmoid Functionally Graded Sandwich Beams in the Framework of High Order Shear Deformation Theory. *Composite Structures*, **276**, Article ID: 114564. https://doi.org/10.1016/j.compstruct.2021.114564